

## Chapter 2

# Physicochemical Properties of Lipids and Macromolecules in Higher Level Organization

**Abstract** This chapter relates in a very concise way, how the physicochemical properties of membrane lipids determine the formation of self-segregated structures. The most common model methods used to understand the influence of lipid organization in membranes, lipid monolayers, liposomes and supported lipid bilayers, are reviewed as well for their suitability in the investigation of lipid-membrane protein interactions.

**Keywords** Langmuir-Blodgett films • Surface phases • Hydrophobic effect • Lipid polymorphism • Liposomes • Guvs • Transition temperature • Fluorescence anisotropy •  $^{31}\text{P}$ -NMR

### 2.1 Lipid Monolayers at the Interface: Two Dimensional Structures

Monolayers formed at the air-water interface are of great interest as earlier exemplified by the work of Gorter and Grendel (see references of Chap. 1) that led to the proposal of a bilayer model for biological membranes. Their insightful and impactful conclusions were, remarkably, based on conventional compression experiments of lipids extracted from red blood cells at the lipid-water interface. Monolayers represent only half of a bilayer but are useful since lateral pressure and physicochemical conditions can be controlled experimentally. Indeed, monolayers have been extensively used to investigate the interaction between proteins, peptides and drugs with lipids and lipid mixtures by mimicking the lipid-water interface of biological membranes.

### 2.1.1 Phases at the Air Water Interface

Monolayers are formed by the deposition of lipids dissolved in a volatile solvent (i.e.  $\text{Cl}_2\text{CH}_2$ ,  $\text{Cl}_3\text{CH}$  or  $\text{CH}_3\text{OH}$ ) at the air-water interface. After a period of solvent evaporation this leads to the spontaneous formation of monomolecular lipid films. Aqueous suspensions and dispersions of lipids such as liposomes will also spontaneously form monolayers at the air-water interface, and the properties of those monolayers provide useful information for understanding the properties of the monolayers and related lipid structures such as liposomes (see, e.g., lung surfactant, below). Conventional experimental set-ups have been derived from pioneering observations that a film could be created in a basic film balance instrument consisting of a cuvette or trough able to contain a subphase where the film was confined between two barriers, one mobile on one end of the trough, and the other floating at the other end. The force exerted by the film on the floating barrier was directly measured by means of a sensitive balance. The designs that are available in modern instruments are based on this earlier approach. Modern troughs are available in different volumes and sizes with one or two mobile barriers made of Teflon to avoid any leakage past the limits of the working surface. When the lipid film is compressed between the two barriers a measure of the *surface pressure* ( $\pi$ ) versus the molecular area ( $A$ ) is obtained. This is normally called a compression isotherm and it is characteristic of the phospholipid (or phospholipid mixture) spread at the air-water interface.  $\pi$  is defined as the difference between the *surface tension* ( $\gamma$ ) of clean surface (water) and that with the monolayer,

$$\pi = \gamma^w - \gamma^m \quad (2.1)$$

Upon lateral compression of a film, the molecular area, referring to the area occupied by a single molecule, decreases in response to the increase in the lateral pressure exerted by the barriers (Fig. 2.1b, c), up to a value of pressure termed the collapse pressure (Fig. 2.1d) where the molecules cannot be further compressed without losing the unimolecular arrangement of the monolayer. At this point during compression both one and two-dimensional phases of the lipid will usually be formed. When monolayers are compressed very slowly, the collapse pressure is usually the same as the equilibrium pressure achieved when lipid suspensions and monolayers coexist over a longer period of time. When monolayers are compressed rapidly, they might enter a metastable one or two-dimensional state, that can relax to the equilibrium pressure over a time that is highly dependent on the composition and the rate of compression (such is the case in lung surfactant).

When kept below their corresponding critical temperatures and surface pressure, phospholipid monolayers can be compressed and may undergo several phase transitions. Four main monolayer phases in two dimensions have been described: the gaseous (G), liquid-expanded ( $L_e$ ), liquid-condensed ( $L_c$ ) and solid (S) phases. Monolayers in the  $L_e$  phase have physicochemical properties similar to those expected of the 3-dimensional  $L_\alpha$  phase (see Sect. 2.6.1). A high degree of care is necessary to obtain an accurate  $\pi$  determination during the operation of these

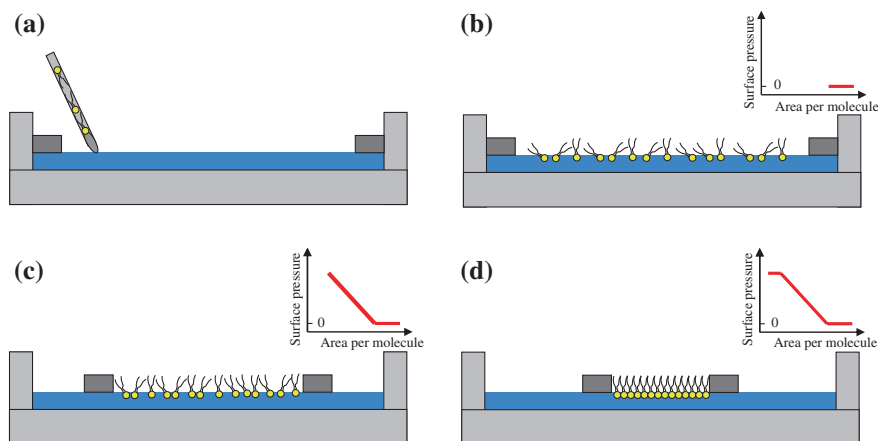


**Fig. 2.1** Cartoon showing the compression with a two floating mobile barriers of a lipid monolayer deposited at the air water-interface and the shapes of the compression isotherms obtained. The surface pressure can be determined by either measuring the force exerted by the film on one of the barriers (original Langmuir method) or by measuring the surface tension in the interfacial film compared to that in the clean solvent (the Lagmuir-Wilhelmy method)

experiments. In biomembrane research, the most common phospholipid used as a reference for isotherm properties is DPPC. This saturated homoacid phospholipid is one of the main constituents of lung surfactant and its compression isotherm (Fig. 2.2) presents very defined and well-established features that can be used as a reference to compare results between laboratories.

At low surface pressures, molecules occupy large areas in such a way that the monolayers can be expanded indefinitely without incurring a phase change. In comparison to what happens with matter in three dimensions, wherein molecules range over large volumes at low pressures, the monolayer is considered to be in G state. After the lateral compression of films of phospholipids in the G phase a  $L_e$  phase appears which is characterized by a decrease in intermolecular distance. Further compression leads to the appearance of an  $L_c$  phase followed by a region of  $L_e - L_c$  phase coexistence, usually characterized by a plateau in the isotherm.  $L_c$  is characterized by maximum packing and a minimum molecular area at the interface. When the lipids have been fully converted to the  $L_c$  phase the surface pressure rises steeply. Further compression of a fully converted  $L_c$  phase, will result in the collapse of the monolayer into three-dimensional forms without further increases in surface pressure. One direct way to visualize the events during compression is the use of fluorescent phospholipid labels like 1-palmitoyl-2-[12-((7-nitro-2-1,3-benzoxadiazol-4-yl)amino)]phosphatidylcholine (NBD-PC) which inserts preferentially into  $L_e$  phase monolayers. The dark domains in Fig. 2.2a–d represent the  $L_c$  phase. As the compression progresses the domains increase in size (after Nag and Keough 1993).

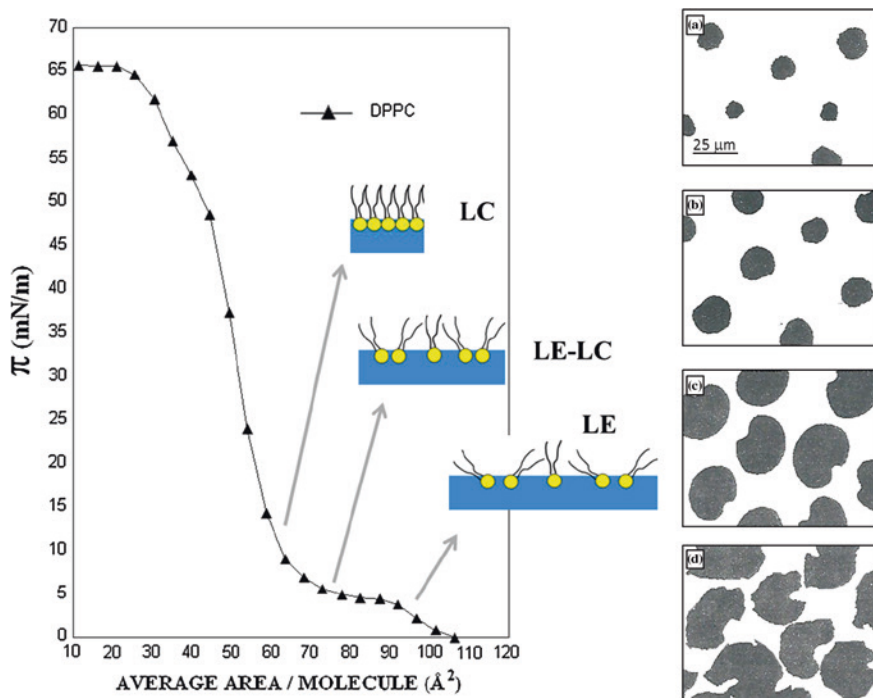


**Fig. 2.2** Surface pressure ( $\pi$ ) as a function of the molecular area of DPPC at room temperature. Cartoons indicate the theoretical disposition at the air-water interface of the molecule. Typical epifluorescence images of the DPPC:NBD-PC (99:1, mol/mol) monolayer at 20 °C at surface pressures of: 4 (a), 7 (b), 10 (c) and 15 (d)  $\text{mN m}^{-1}$

### 2.1.2 Monolayer Compressibility

The *compressibility* ( $C_s$ ) of a monolayer is defined by

$$C_s = -\frac{1}{A} \left( \frac{\partial A}{\partial \pi} \right)_{T,n} \quad (2.2)$$

where  $A$  is the molecular area of the phospholipid. It can be calculated from the slope of the curve of  $\pi$  versus the molecular area. Often it is expressed as the reciprocal of the *compressional modulus*  $C_s^{-1}$  that is

$$C_s^{-1} = (-A) \cdot \left( \frac{\partial \pi}{\partial A} \right)_{T,n} \quad (2.3)$$

In practical terms, the derivative of the experimental data is computed by fitting a straight line to a window of an area width of  $\sim 0.2 \text{ nm}^2 \text{ mol}^{-1}$  around any given

surface pressure value, so that experimental noise is filtered out. It follows that the  $C_s^{-1}$  value for the clean air-water interface is zero, with an equivalent value being found experimentally for monolayers in G state; its value ranges between 5 and 50 mN m<sup>-1</sup> for the  $L_e$  state and between 100 and 250 mN m<sup>-1</sup> for the  $L_c$  state. Solid state compressional moduli may range from 1000 up to 2000 mN m<sup>-1</sup> (Davies 1963).

### 2.1.3 Mixing Properties of the Monolayers at the Interface

The determination of mixing properties of lipids in monolayers can help in understanding their mixing properties in bilayers or membranes. Most useful in this regard is determining the magnitudes of the thermodynamic characteristics associated with the process. The molecular area of an ideally mixed monolayer of two components can be calculated according to

$$A^{id} = \chi_1 A_1 + \chi_2 A_2 \quad (2.4)$$

where  $A^{id}$  is the monolayer and  $\chi_1, A_1$  and  $\chi_2, A_2$  are the molar fractions and the molecular areas of the pure components 1 and 2, respectively. The excess area,  $A^E$ , for a binary monolayer can be expressed as follows

$$A^E = A_{12} - (\chi_1 A_1 + \chi_2 A_2) \quad (2.5)$$

where  $A_{12}$  is the molecular area of the mixed monolayer. Negative values of  $A^E$  indicate attractive forces between molecules while positive values indicate repulsive forces. The interaction between two phospholipid components in a mixed monolayer, at a constant  $\pi$  and temperature, can be evaluated by calculating the excess *Gibbs energy* ( $G^E$ ), which is given by

$$G^E = \int_0^\pi [A_{12} - (\chi_1 A_1 + \chi_2 A_2)] d\pi \quad (2.6)$$

$G^E < 0$  means that the mixing between both components is favored and, conversely  $G^E > 0$  indicates that mixing of molecules is disfavored. The meaning of  $G^E$  can be better understood by defining the *Gibbs energy of mixing* as follows

$$\Delta_{mix} G = \Delta_{mix} G^{id} + G^E \quad (2.7)$$

where the first term, the ideal Gibbs energy of mixing ( $\Delta_{mix} G^{id}$ ), can be calculated from the equation

$$\Delta_{mix} G^{id} = RT(\chi_1 \ln \chi_1 + \chi_2 \ln \chi_2) \quad (2.8)$$

where  $R$  is the universal gas constant and  $T$  is the temperature. We find that  $G^E$  at a defined temperature depends on the magnitude of available experimental conditions of composition and intrinsic molecular areas. All these thermodynamic

magnitudes will vary when there are interactions between peptides or proteins in the monolayer.

## 2.2 Langmuir-Blodgett Films

Langmuir-Blodgett (LB) techniques (Petty 1996) were developed in the first decades of the twentieth century. The strategy consisted of raising a solid substrate through a monolayer that was formed at the interface as is depicted in diagrams in Fig. 2.3a–c. If the substrate is hydrophilic the headgroups become attached onto the substrate with the acyl chains facing the air as it passes upward (upstroke). Conversely, by using a hydrophobic substrate and passing it downward (downstroke) through the phospholipid monolayer, the acyl chains will be attached onto the solid surface and the headgroups will face the water subphase. The technique has the advantage that ionic strength, pH, temperature and surface pressure can be kept constant in such a way that the monolayer is theoretically transferred onto the substrate with the same structural properties that it had at the air-water interface. The transfer ratio (TR) value gives information about the yield of coverage of the solid substrate, it being nearly 1 for a fully effective transfer. In this way a lipid monolayer can be transferred at any desired point of the isotherm (Fig. 2.2) and the features of the different states (i.e.  $L_e$  or  $L_c$ ) can be scrutinized by using suitable surface imaging techniques (i.e. XPS or AFM). A point of criticism may arise from the possible difference between the lateral surface pressure at the air-water interface and the lateral pressure in the transferred LB film. Although, many mechanical aspects such as the lifting speed have been improved over the years, it is true that the transferred LB film might be a little more relaxed, i.e., at a slightly lower lateral pressure or packing density than the film from which it was transferred.

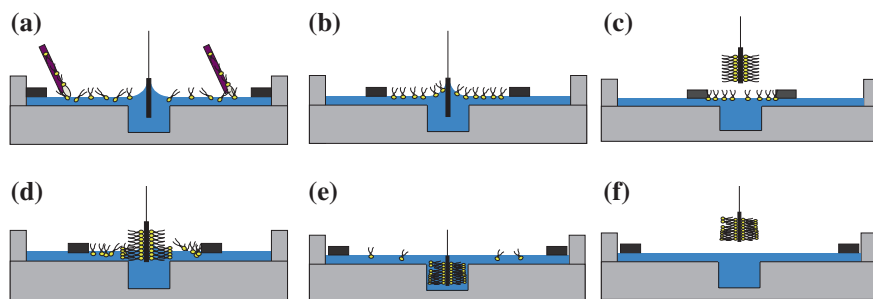


**Fig. 2.3** Langmuir-Blodgett extraction: lipids are spread at the air-water interface (a) and compressed to the desired surface pressure (b). A first monolayer is extracted by lifting up a substrate through the interface (c), followed by passing the substrate downward into the subphase to attach a second monolayer (d, e). Subsequent rising of the substrate (f) produces a substrate that is coated with a double monolayer or bilayer

The LB technique can be further exploited to obtain bilayers by double monolayer deposition. The procedure may be performed as follows: the lipids of interest are spread at the air-water interface and at the convenient surface pressure transferred onto a solid hydrophilic support. Afterwards, a second monolayer is transferred onto the one deposited before on the down-stroke to obtain a supported bilayer (Fig. 2.3c–e). The technique can be used to obtain asymmetric bilayers with different surface pressure at the apical and distal monolayers of the bilayer, with the same or different composition.

## 2.3 Structures at the Air-Water Interface

Several direct optical methods applied at the air-water interface or indirect methods applied to the extracted LB films, can be used to investigate the structure of the lipid films. The first direct visual evidence of a  $L_e$ - $L_c$  phase equilibrium was provided by fluorescence microscopy of monolayers (FM) (Peters and Beck 1983) which is based on the different affinity of fluorescent phospholipid analogs for the different phases. A drawback of FM is that the presence of fluorescent phospholipid analogs used as reporters induced some distortions in the packing structure of the phases, so that the concentration of probe in the monolayer (or bilayer) needs to be kept as low as practically possible. Different techniques for studying monolayers without the use of probe molecules have become available. These include Brewster angle microscopy (BAM) (Hoenig and Moebius 1991), atomic force microscopy (AFM), X-ray reflectivity and ellipsometry, and surface Raman spectroscopy. It is worth noting that distortions and artefactual behavior can easily occur in all monolayer measurements, and great care is necessary in both experimental execution and the interpretation of results.

### 2.3.1 Brewster Angle Microscopy

BAM is a microscopic method based upon the absence of reflection of p-polarized light from a clean interface at a certain angle (Brewster angle). When lipids are incorporated into the air-water interface the refractive index varies and the covered part of the surface reflects light at the Brewster angle for the clean surface. The different monolayer phases have different reflectances so BAM is capable of providing information on the  $L_e$ - $L_c$  transitions in lipid monolayers along with information about domain morphology and the possible order and local packing of the domains. As an example the surface pressure-area ( $\pi$ -A) isotherm of a pure POPE monolayer at  $24.0 \pm 0.2$  °C is shown in Fig. 2.4 along with BAM images taken at different surface pressures (Domènech et al. 2007a). At very low surface pressures the monolayer is in the G state (Fig. 2.4a). While the isotherm of POPE is in the  $L_e$  phase, BAM images reveal the existence of bright spots (Fig. 2.4b). Their number does not appear to increase above  $\pi \sim 6$  mN m<sup>-1</sup>, although they

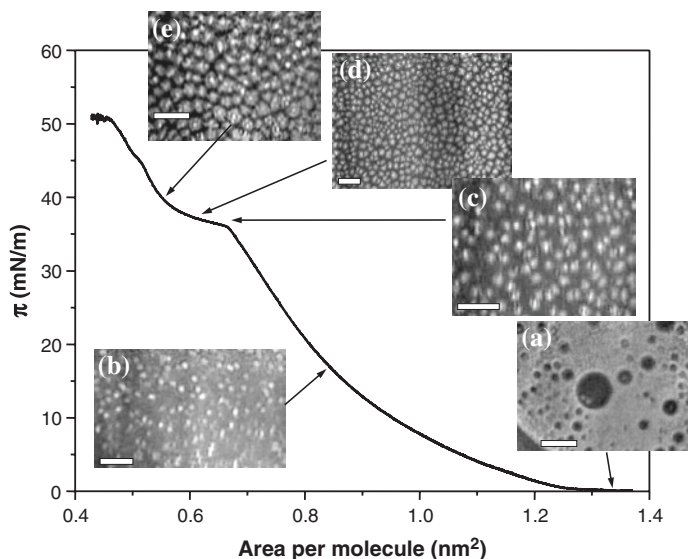


**Fig. 2.4** Compression isotherm of POPE showing the typical  $L_e$ - $L_c$  coexistence plateau that extends from  $\sim 0.68$  to  $\sim 0.57$  nm<sup>2</sup> mol<sup>-1</sup> and the collapse at 50.7 mN m<sup>-1</sup>. BAM images were captured at 0.5 (a), 15 (b), 36 (c), 38 (d) and 39 (e) mN m<sup>-1</sup>. Adapted with permission from Domènech et al. (2007a) © 1997. American Chemical Society

become increasingly brighter upon compression. Images do not reveal any new emerging structures until the plateau region when the growth of globular domains with increased BAM reflectivity is observed (Fig. 2.4c, d) which is consistent with a  $L_e$ - $L_c$  phase transition. Bright spots present at lower pressures act as nucleation points of the new domains, whose structure is typical of condensed  $L_c$  domains in phospholipid monolayers. The major drawback of BAM is the limited resolution, which falls within the range of micrometers. In this regard, it could be of interest to compare BAM with AFM images of the same monolayer.

### 2.3.2 Atomic-Force Microscopy (AFM)

AFM is a near-field microscopy technique forming part of the wider group of scanning probe microscopy techniques (SPMs), which were developed after the invention of scanning tunneling microscopy (STM) by Binnig et al. (1982). AFM provides outstanding vertical and lateral resolution (better than 0.1 nm and 1 nm, respectively). AFM scanning of POPE monolayers complements the previous BAM observations. The POPE isotherm is presented in Fig. 2.5 along with AFM images of LBs extracted at different surface pressures.

The LB extracted at 10 mN m<sup>-1</sup> (Fig. 2.5a) is featureless and corresponds to the  $L_e$  phase. At 30 mN m<sup>-1</sup> numerous randomly distributed vacancies with



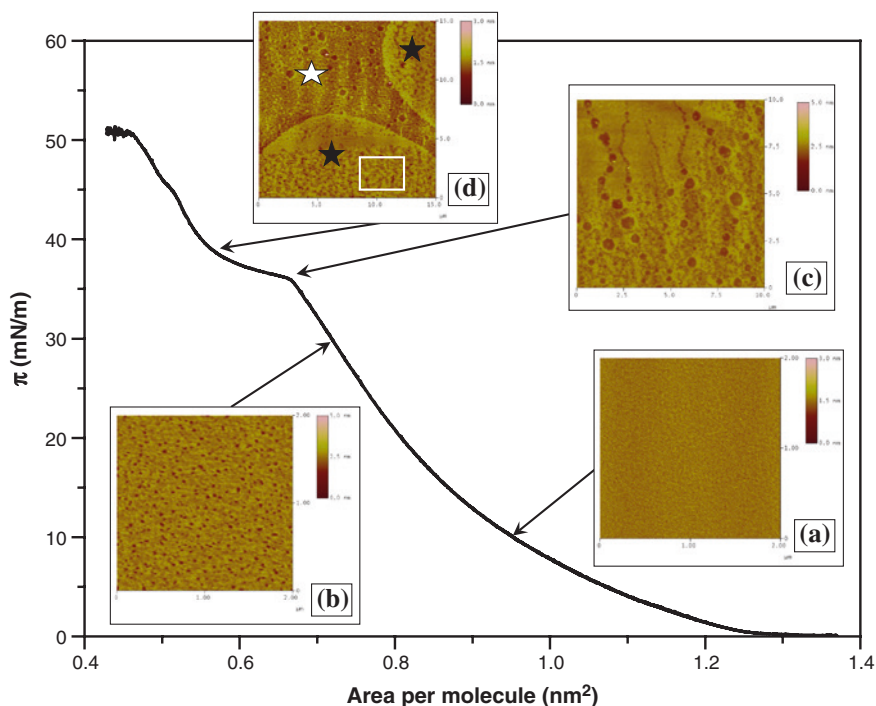


**Fig. 2.5** Compression isotherm of POPE showing the typical  $L_e$ - $L_c$  coexistence plateau that extends from  $\sim 0.68$  to  $\sim 0.57$  nm<sup>2</sup> mol<sup>-1</sup> and the collapses at 50.7 mN m<sup>-1</sup>. AFM images were acquired at 10 (a), 30 (b), 36 (c) and 39 (d) mN m<sup>-1</sup>. Adapted with permission from Domènech et al. (2007a) © 1997. American Chemical Society

a diameter of  $\sim 75$  nm are observed (Fig. 2.5b). As surface pressure increases these vacancies coalesce resulting in regions with diameters ranging from  $\sim 90$  to  $\sim 500$  nm at 36 mN m<sup>-1</sup> (Fig. 2.5c). When the pressure reaches 39 mN m<sup>-1</sup>, these vacancies have grown into much more complex structures (Fig. 2.5d). This last image shows two well defined domains with a step-height difference of  $\sim 0.5$  nm that represents the typical step height between  $L_c$  and  $L_e$  phases. The thinner domain (white star) represents the  $L_e$  and the thicker domain (black star) represents the  $L_c$  phase. It is worthwhile mentioning that the LC structures are of a similar size as those observed in Fig. 2.3e.

## 2.4 Protein- and Peptide-Lipid Interactions in Monolayers

Different experimental approaches can be used to investigate the interaction between proteins and peptides with lipid monolayers. One experimental approach used to determine the nature of the interaction has been to inject the molecule of

interest into the subphase beneath the lipid monolayer. Molecules that have some hydrophobic components such as peptides or proteins that are dissolved in aqueous solutions, will display some tendency to migrate into the air-water interface. They will “compete” for surface space with lipids in very loosely packed monolayers. Subsequent compression of the mixed monolayers can yield useful information about the thermodynamics of the mixed lipid-protein/peptide film. If there is insertion of the protein or peptide into the lipid monolayer there will be changes in the isotherms obtained by compression of the film. Usually, moderate expansions to larger nominal lipid molecular areas are observed most likely due to the intercalation of the peptide or protein between the lipid molecules. In some instances, the insertion leads to a condensation of the film to lower nominal molecular areas per lipid. The repulsive or attractive manner of the interaction can be quantitatively evaluated within the surface thermodynamics framework described in Sect. 2.1.3. Protein or peptide molecules do not need to insert into the film to have an influence on the lipid packing. Some molecules may interact with or attach to the headgroup region of the phospholipids causing effects on the isotherms. In some cases, especially when the protein or peptide is itself highly amphipathic, it can cause desorption of the lipid monolayer into the subphase by the formation of micelles.

Another simple and common method used in peptide research consists of following the adsorption of the molecules of interest into the air-water interface containing a lipid monolayer at constant area and recording the changes in the surface pressure as a function of the time. The interaction can be also measured, as will be discussed in Sect. 2.4.4, by keeping the surface pressure constant while measuring the increase or decrease of the area covered by the monolayer as an indicator of the interaction (Maget-Dana 1999).

### 2.4.1 Interfacial Studies for Understanding Enzyme Activity

Lipid monolayers are used as model membranes. They can also be exploited to investigate the action of soluble enzymes such as phospholipases (PLs), on specific phospholipids, a process which was pioneered by the De Haas Group in the 60s and 70s (Verger et al. 1973). PLs hydrolyze phospholipids at the membrane interface liberating fatty acids and for this reason the monolayer is a well suited membrane model for the investigation of the molecular mechanism of action of PLs.

Members of the extracellular secretory phospholipase A<sub>2</sub> family (PLsA<sub>2</sub>) are the most extensively studied enzymes that catalyze reactions at the lipid-water interface. PLsA<sub>2</sub> catalyze the hydrolysis of the *sn*-2 ester bond of glycerophospholipids leading to free fatty acids and lysophospholipids. PLsA<sub>2</sub> undergo a significant increase in their catalytic activity when bound to the surface of phospholipid membranes, a process highly sensitive to some membrane physical properties such as phase, surface charge or curvature. A model for the action of PLsA<sub>2</sub> at interfaces was proposed by Verger et al. (Fig. 2.6). This model which basically consisted of two successive equilibria: the first describing the interfacial adsorption and penetration

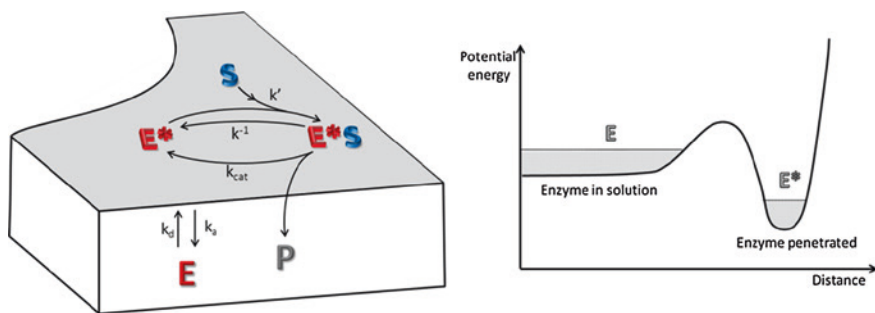


**Fig. 2.6** Reaction mechanism of a soluble enzyme with a lipid substrate at an interface

of  $PLsA_2$  into the phospholipid monolayer, which leads to an activated form of the enzyme; and the second, describing the formation of the activated enzyme-substrate complex following the Michaelis–Menten model adapted to two dimensions.

### 2.4.2 Adsorption of Soluble Proteins to Lipid Monolayers

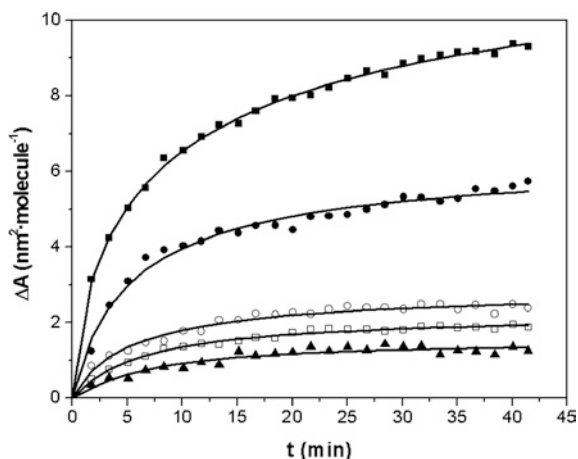
A good example of these experiments is cytochrome *c* (cyt *c*), a peripheral membrane protein that is localized at the inner membrane of mitochondria. It is an essential component of the mitochondrial respiratory chain, transferring electrons between the  $CoQH_2$ -cytochrome *c* reductase and the cytochrome *c* oxidase complexes. The mechanism by which cyt *c* diffuses between the reductant and the oxidant protein substrates may involve translational motion of cyt *c* in the two-dimensional plane defined by the bilayer, with the protein interacting specifically with cardiolipin (diphosphatidylglycerol).

One can study the interaction and insertion of soluble proteins with lipid monolayers by monitoring the increase in nominal area per lipid molecule at constant surface pressure as a function of time after injecting the protein below the lipid film. In Fig. 2.7, an example of such an experiment where cyt *c* was injected beneath lipid monolayers of different composition held at constant surface pressure is shown. In these experiments,  $\pi$  was kept at  $30 \text{ mN m}^{-1}$  while cyt *c* was injected to reach a final concentration of  $2 \text{ }\mu\text{M}$ . Changes of surface molecular area ( $\Delta A$ ) with time ( $t$ ) are measured and experimental data fitted to the a Langmuir-derived isothermal adsorption equation

$$\Delta A = \Delta A_{\max} \frac{(k_i t)^b}{1 + (k_i t)^b} \quad (2.9)$$

where  $\Delta A_{\max}$  is the maximum increase of the lipid molecular area reached in steady-state conditions,  $k_i$  is a rate constant determined by the nature of the substances involved and the experimental conditions, and  $b$  is a parameter that is

**Fig. 2.7** Increase of the surface area  $A$  as function of time of monolayers after subsurface injection of cyt  $c$ : CL (■), POPE (□), POPC (○), POPE:CL (0.8:0.2, mol/mol) (●), and POPC:CL (0.6:0.4, mol/mol) (▲). Reprinted with permission from Domènech et al. (2007a, b, c). *Langmuir*. 23 (10):5651–6. © 1997. American Chemical Society



related to the cooperativity of the process. What Fig. 2.7 implies is that while the interaction between cyt  $c$  and pure zwitterion phospholipids (POPE and POPC) involves a hydrophobic contribution, the presence of an anionic phospholipid (for instance CL) in the POPE monolayer enhances the penetration of cyt  $c$  which can be attributed to specific electrostatic interactions.

### 2.4.3 Peptide Interaction with Monolayers

An initial recognition between a (soon to be infected) host-cell and a microbial pathogen must take place. This recognition occurs between transmembrane proteins (receptors) present in the membranes of the host-cell and the pathogen, or between pathogen membrane receptors and the outer leaflet moiety of the host-cell membranes. The biophysical study of these interactions using lipid monolayers can shed light into the mechanism of the infection processes. Regrettably, transmembrane proteins are only stabilized in water solution in the presence of surfactant molecules that form micelles or other three-dimensional structures (e.g. bicelles) around the proteins, shielding their hydrophobic moieties. Notably, this handicap has been successfully solved in many cases by a “divide and conquer” strategy consisting of studying only the specific parts of transmembrane proteins (normally peptides that can be obtained synthetically) known to be the key elements in the interactions with lipid membranes.

In these types of experiments the selected peptides must themselves possess surface activity. Initially, the saturating concentration of these peptides is set to where no further increase in surface pressure can be obtained. Thereafter any further increase in concentration can be determined by performing surface pressure measurements at increasing peptide concentrations in absence of a lipid monolayer. Next, maximum insertion pressures (MIPs) for a defined lipid monolayer

and peptide combination are determined by injecting the peptide underneath the lipid monolayer at different initial pressures ( $\pi_i$ ). In these experiments when the peptide-lipid monolayer interaction reaches an equilibrium, a new surface pressure ( $\pi_e$ ) is attained. Performing experiments at increasing  $\pi_i$  values yields a representation of the surface pressure increase  $\Delta\pi$  ( $\Delta\pi = \pi_e - \pi_i$ ) as a function of  $\pi_i$ . The value for the MIP can be determined from this curve as the intersection point with the x-axis. It is believed that membrane lateral pressure in biological membranes varies from 25 to 30 mN m<sup>-1</sup> so MIPs values below these numbers will suggest that peptides cannot penetrate the monolayer. Interestingly, the affinity between the lipid monolayer and the peptides can be calculated by adding 1 to the slope of the curve of  $\Delta\pi$  as a function of  $\pi_i$ . Negative and positive synergy values represent repulsive and attractive interactions between lipids and peptides, respectively. A zero value represents no interaction.

#### 2.4.4 The Membrane Associated Surfactant Proteins

Lung surfactant is a lipid-protein complex located in the aqueous lining layer of the lung and at the air-water alveolar interface with the principal physiological function of regulation gas exchange activity between the airspaces of the lung and the blood (Pérez-Gil 2008). Lung surfactant also participates in the defense against inhaled pathogens and modulates the function of respiratory cells. It is found in the air spaces in different physical forms with different biophysical activities and with attendant small changes in composition. Pulmonary surfactant is synthesized, assembled and secreted onto the respiratory surface by specialized cells of the alveolar epithelium. It reduces the surface tension of the thin layer of water that covers the lung epithelium. It reduces the work of expansion of the lung surface and it prevents the collapse of the alveoli during expiration. Lack of an operative surfactant system is associated with severe respiratory dysfunction. Lung surfactant has a very particular composition and organization that has been extensively investigated by means of monolayers since it is accepted that the physiological function of lowering surface tension is achieved by a monolayer at the lung air-water interface, possibly associated with adjacent or adhering bilayer structures. More recently techniques that capture the properties of the lung *in vivo* such as the captive bubble method have also been used to study this complex system (Schurch et al. 1992).

Although the composition may vary between species and according to environmental and pathological conditions, lung surfactant is composed of 90 % lipids by weight and 10 % proteins. DPPC is by far the most abundant lipid species in mammalian lung surfactant and usually accounts for 50 % or more of the lipid component. It is essential for producing the very low surface tension (DPPC has a high surface pressure according to Eq. 2.1) observed during lung exhalation which corresponds to surface area reduction and compression of a monolayer at the lung surface. This property is directly related with its saturated acyl chains (16:0),

which can adopt a highly packed lateral state (Fig. 2.2). Other species such as PG or PI account for less than 10 % by weight of the total lipid fraction of lung surfactant. The presence of a relatively high PG content in surfactant is unique for this lipid in any mammalian system or membrane. These negatively charged species are thought to participate in selective interactions with cationic hydrophobic proteins. Cholesterol is a significant component, constituting up to about 15 % of the lipid on a molar basis. Lung surfactant also contains four specific proteins, two of them, SP-A and SP-D, are hydrophilic, and the other two, SP-B and SP-C, hydrophobic. The two hydrophobic proteins interact strongly with lipids. Even the two hydrophilic proteins show some propensity to interact with lipids. Their structural models and proposed mode of interaction in the alveolar spaces are presented in Fig. 2.8. SP-B and SP-C participate in the surface activity of the surfactant, while SP-A and SP-D play a major role in innate immune defense in the lung.

SP-B is a small protein (a homodimer of 8.7 kD monomers) with approximately 40 % of its amino acids of hydrophobic nature and with 30–45 %  $\alpha$ -helical secondary structure. SP-B contains seven C residues, six of them forming three intramonomer disulfide bonds and one establishing an intermonomer disulphide bridge that yields a covalent homodimer. The distribution of polar and non-polar amino acids in the  $\alpha$ -helices renders them amphipathic along their helical axis.

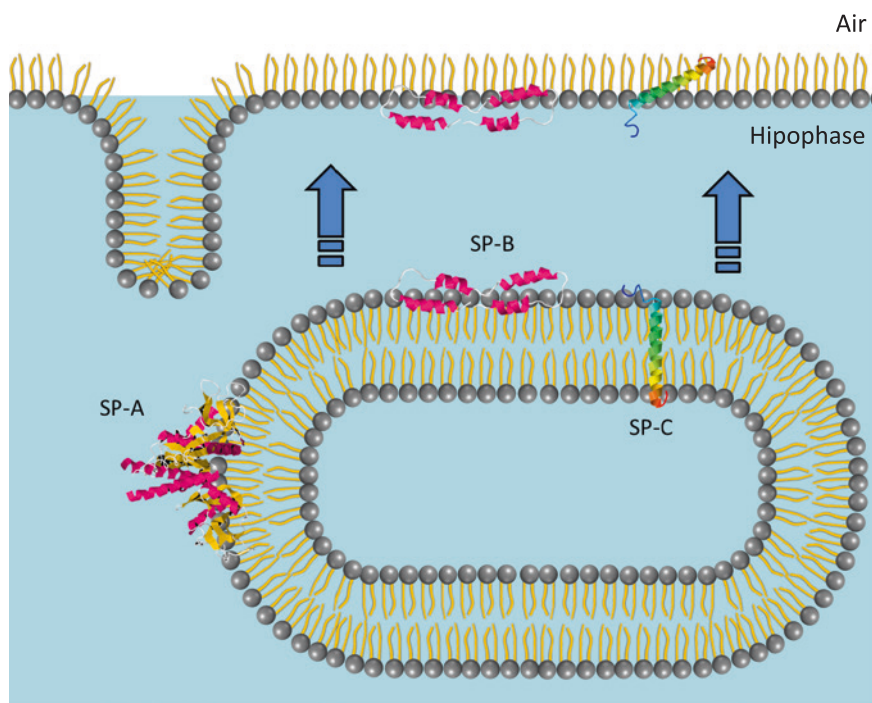


**Fig. 2.8** Current models on the structure and orientation of the three proteins usually obtained associated with pulmonary surfactant membranes, SP-A, SP-B and SP-C. Adapted by permission of from Pérez-Gill (2008)



This sort of arrangement is often found in proteins that interact peripherally with membranes or which can form hydrophilic channels in membranes. SP-B appears to behave like a tightly bound peripheral membrane protein. It forms two types of interactions with phospholipids. The basic residues of the SP-B helices are proposed to form ionic interactions with PG in the phospholipids, and the hydrophobic portions of the helices interact with the hydrophobic parts of the phospholipids. These interactions are thought to be essential for the role of SP-B in the surfactant interfacial adsorption of phospholipids.

SP-C is also a small hydrophobic protein (3.7 kDa) with a  $\alpha$ -helical secondary structure (about 70 %) as well (see Fig. 2.8). The N-terminal segment of SP-C has a positive net charge and includes two palmitoylated cysteine residues. These palmitic acyl chains are essential to anchor the N-terminal segment of SP-C into the membrane. The C-terminal region is enriched in branched aliphatic residues forming an  $\alpha$ -helical motif, which spans the bilayer. In the membrane, SP-C is tilted  $\sim 70^\circ$  respect to the membrane plane, exposing the positive charges and allowing for the establishment of preferential interactions with anionic phospholipids.

SP-A and SP-D are hydrophilic proteins that are components of the innate immune system. They modulate the inflammatory response involved in removing pathogens from the epithelial surfaces. They recognize numerous types of microorganisms, including viruses, bacteria, and fungi. SP-A and SP-D contain specific regions that are able to bind different carbohydrate domains present on pathogenic surfaces. In addition, SP-A can bind DPPC through these regions. This is an interaction that is suggested to be critical for the formation of tubular myelin (a unique and regular network of membranes extended by the surfactant at the airways). The N-terminal sequences of SP-A and SP-D seem to be necessary not only for oligomer stabilization, but also for the interaction with phospholipids and the formation of tubular myelin.

## 2.5 Structures of Lipids in Aqueous Environments

Phospholipids are said to be mesomorphic in that they can exist in several organizational forms, both in pure forms and when they are dispersed in aqueous environments. As discussed in Chap. 1, all phospholipids are amphiphilic compounds that contain a polar region and a hydrophobic region, but their behavior in aqueous environments varies considerably (Gennis 1989). They take up different phases wherein the fundamental lipid structures can be simplified into shapes as shown in Fig. 2.9.

While lipids exhibiting an inverted truncated cone-shape with small head group tend to adopt the hexagonal inverted structure,  $H_{II}$ , species such as lysophospholipids and many detergents, with a relative small headgroup and often with only one acyl chain, tend to adopt a cone shape,  $H_I$ . In turn, lipid molecules with cylindrical shape, such as PC or SM, are likely to adopt the structure of a bilayer. Intralipid moieties such as the nature of the polar group and the chain length and degree of acyl chain unsaturation will influence the shape and the tendency to

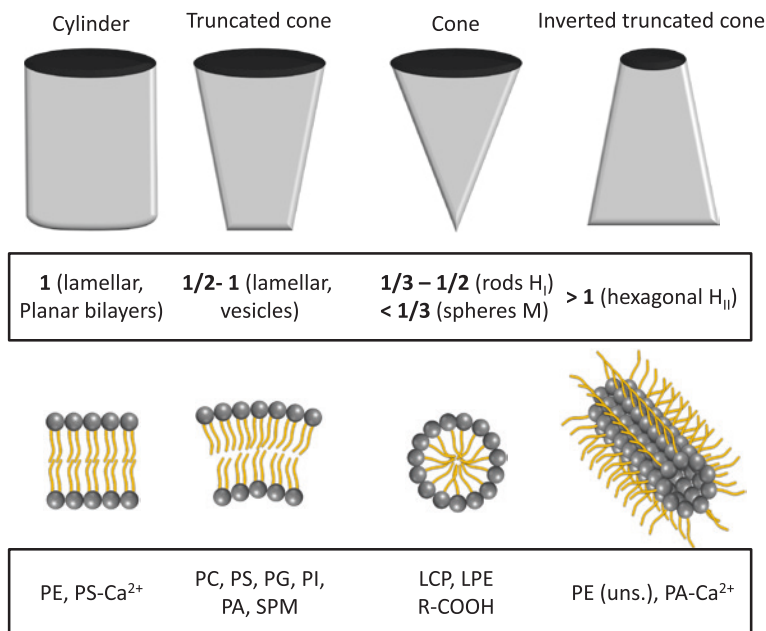


**Fig. 2.9** Molecular shapes and the critical packing parameter for some membrane lipids. Redrawn after Gennis (1989)

form different phases. A so-called critical packing parameter ( $P$ ) was introduced to rationalize this phenomenological behavior (Israelachvili et al. 1976)

$$P = \frac{v}{S_o l_c} \quad (2.10)$$

where  $v$  is the molecular volume,  $S_o$  the optimal or equilibrium surface area of the polar group at the interface of the aggregate and  $l_c$  the chain length.  $P$  can then be used to predict the preferred association structure based on the geometrical parameters of the amphiphile. When  $P \leq 1/3$ , a micellar sphere is expected; when  $1/3 \leq P \leq 1/2$  cylindrical micelles are likely to occur; when  $1/2 \leq P \leq 1$  the formation of bilayers is favored and when  $P > 1$ ,  $H_{II}$  phases are formed.

$P$  is a geometrical parameter expressing the intrinsic curvature of a phospholipid species as defined in 2.10 by the ratio of the diameter of the head group to that of the acyl chains. As we will discuss in Sects. 3.4 and 3.5 the spontaneous curvature of lipids, referring to their natural tendency to bend in the most thermodynamically stable conformation, plays a crucial role in the lipid-IMP interaction. The spontaneous curvature, indicated by  $c_o$  and expressed in  $\text{nm}^{-1}$  describes the tendency to adopt a curved conformation, positive or negative and is dependent of the headgroup-acyl chain balance.  $c_o = 0$  for cylindrical formed lipids,  $c_o < 0$  for lipids with tail region bigger than the headgroup and, conversely,  $c_o > 0$  for lipids with tail region smaller than the headgroup. For instance, negative  $c_o$  values



will be found for POPE, DOPE or CHOL and positive  $c_o$  values will be found for POPC, DPPC or DSPC. As will be discussed in Chap. 4, it is known that the curvature of lipid monolayers plays a crucial role in the activity of several IMPs.

### 2.5.1 Hydrophobic Effect and Lipid Self-aggregates

The solubility of lipids in water is very low due to unfavorable hydrophobic interactions of the acyl chains with water. The solubility depends on the temperature, and the length and size of the acyl chains. Many surfactants, such as soaps detergents or bile salts, have a significant solubility in water as monomers. When their concentrations are increased, they spontaneously form small aggregates called micelles, which can exist in equilibrium with the monomers. The formation of micelles occurs for each amphiphile at a defined solute concentration, called the critical micellar concentration (CMC). Below the CMC the amphiphilic molecules tend to migrate to the air-water interface (Fig. 2.10) with the acyl chains oriented to the less apolar phase, that is, the air. For other amphipathic compounds with a higher hydrophobic to hydrophilic nature such as a phospholipid, monomer concentrations can be vanishingly small, and larger aggregate structures are formed at very low concentrations.

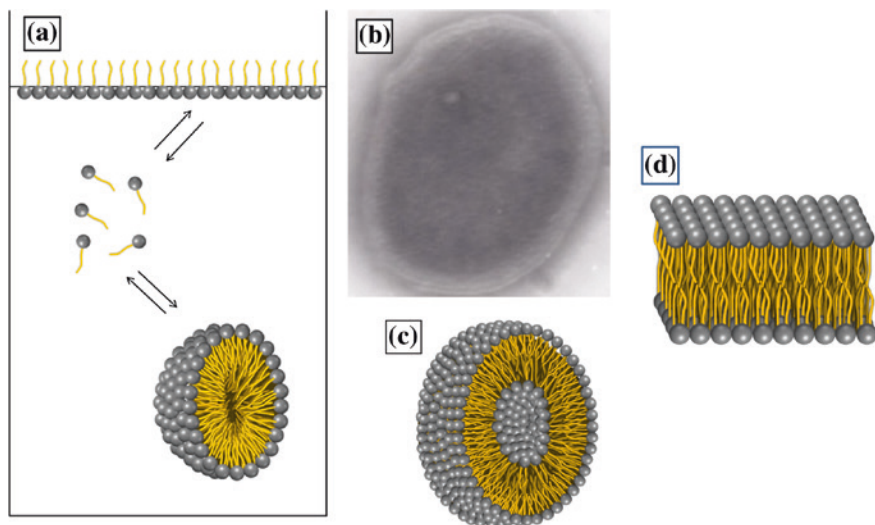


**Fig. 2.10** At small concentrations of surfactant, monomers tend to migrate to the air water interface and when the concentration is  $\sim$ CMC, micelles are formed beneath the monolayer (a). Multilamellar liposomes stained with phosphotungstic acid as observed by EM (b); cartoon of a unilamellar liposomes (c); and a planar lipid bilayer (d)

The aggregation into these macromolecular structures results from the hydrophobic effect. This refers to the association of the hydrophobic moieties of molecules in order to avoid an aqueous environment. This leads to the formation of structures with the hydrophilic headgroups facing the aqueous environment and the hydrophobic groups in self-aggregated arrays.

Segregation of amphiphiles into micelles or bilayers can be described by means of thermodynamic analysis. The chemical potential of an amphiphile can be expressed as

$$\mu_i = \mu_i^\circ + kT \ln \chi_i \quad (2.11)$$

where  $\mu_i^\circ$  is the standard state chemical potential of species  $i$  in solution,  $\chi_i$  the mole fraction,  $k$  the Boltzmann constant and  $T$  the temperature. In a solution of amphiphiles we can find several aggregation states in equilibrium, from the monomeric form to the structure with the maximum number ( $N$ ) of aggregated molecules. Hence, the chemical potential can be expressed as

$$\mu_N = \mu_N^\circ + \frac{\kappa T}{N} \ln \left( \frac{\chi_N}{N} \right) \quad (2.12)$$

where  $\mu_N^\circ$  is the standard state chemical potential of the species with a number  $N$  of molecules. Three terms have been postulated (Gennis [1989](#)) to contribute to the value of  $\mu_N^\circ$  according the following equation

$$\mu_N^\circ = \gamma S + \frac{C}{S} + G_N \quad (2.13)$$

where  $\gamma$  is the interfacial surface tension,  $S$  the average surface area,  $G_N$  the Gibbs energy associated with the acyl chains and  $C$  is a constant. The first two terms are attractive and repulsive, respectively, whilst the third one is defined as an energetic term associated with the acyl chains. The first two terms account for the energetic contribution due to the intermolecular interactions at the water-hydrocarbon region. Notice that the optimal surface area ( $S_o$ ) can be easily obtained by setting  $d\mu_N^\circ/dS = 0$  which gives  $S_o = (C/\gamma)^{1/2}$ . This relationship shows that the value of  $S_o$  depend on  $C$ , the repulsion constant, in such a way that larger values of  $C$  result in larger values of  $S_o$ .

If we assume an equilibrium between the monomeric state ( $N = 1$ ) and the micelle state with the maximum number of aggregation  $N$ , we can accordingly write from the phase equilibrium rule that

$$\mu_1^\circ + kT \ln \chi_1 = \mu_N^\circ + \frac{kT}{N} \ln \left( \frac{\chi_N}{N} \right) \quad (2.14)$$

and rearranged it in the following way

$$\mu_N^\circ - \mu_1^\circ = kT \ln \chi_1 - \frac{kT}{N} \ln \frac{\chi_N}{N} \quad (2.15)$$

The difference between the standard states of the chemical potentials can be interpreted as the hydrophobic Gibbs energy because of the exclusion of water from

the apolar region of the amphiphile when the aggregate is formed. More intuitively,  $\mu_N^\circ - \mu_1^\circ$  is the Gibbs energy required to transfer a monomer to the aggregate in such a way that the more negative this energy is the smaller  $\chi_N$  will be. In other words, from Eq. 2.15 it can be inferred that the concentration of the lipid in the aggregated form, the  $\chi_N$  increases when the difference in the standard chemical potentials increase.

### 2.5.2 Liposomes

Liposomes were initially described as closed structures consisting on a large number of concentric bilayers that were formed upon the hydration of phospholipids (Bangham et al. 1965). Over the subsequent 50 years the great utility of liposomes prepared by the hydration of natural or synthetic phospholipids as model membranes and drug delivery systems, among other uses has been demonstrated by their use in tens, if not hundreds, of thousands of experiments. When dry phospholipids are dispersed in water, multilamellar vesicles (MLVs) (Fig. 2.10) are formed spontaneously. By using the appropriate techniques the size of the liposomes can be controlled. Typically they are classified as small unilamellar vesicles (SUVs; 20–100 nm), large unilamellar vesicles (LUVs; 100–500 nm) and giant unilamellar vesicles (GUVs; 0.5–100  $\mu\text{m}$ ).

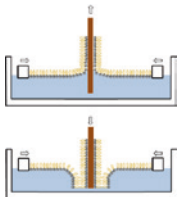
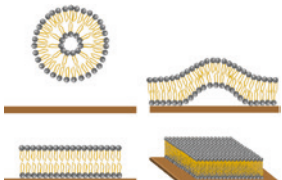
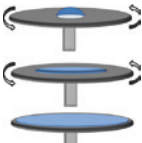
### 2.5.3 Supported Membrane Systems

The increasing interest in confining lipid bilayers on solid surfaces for investigation has led to a number of supported membrane systems, including supported lipid bilayers (SLBs), polymer-cushioned lipid bilayers, hybrid bilayers, tethered bilayers, suspended lipid bilayers and supported vesicular layers (Groves and Boxer 2002; Tanaka and Sackmann 2005). In addition to the above mentioned Langmuir-Blodgett (LB) and Langmuir-Schaefer (LS) double deposition methods (Petty 1996), the foremost methods for obtaining SLBs involve the spreading of liposomes and the spin coating of lipids onto preconditioned supports (Simonsen and Bagatolli 2004) (Table 2.1).

### 2.5.4 Giant Unilamellar Vesicles (GUVs)

Giant unilamellar vesicles (GUVs) (Fig. 2.11) have been widely used in the study of membrane nanomechanics, and more recently in the investigation of lateral segregation of membrane components. GUVs have diameters between 5 and 200 micrometers and for this reason are suitable for optical techniques such as

**Table 2.1** Summary of the common methods used to prepare SLBs: Langmuir-Blodgett/Langmuir Schaeffer deposition, vesicle fusion and spin coating, together with the main advantages and disadvantages of each technique. The table provides selected references for further information and a schematic diagram of the corresponding method (Picas et al. 2012)

General methods to prepare SLBs			
			
	Langmuir-Blodgett/ Langmuir Schaeffer deposition	Vesicle fusion	Spin coating
Advantages	Asymmetric bilayers (in composition and lateral pressure)	Simplicity (in terms of manipulation)	Full coverage Absence of defects Single or multi-bilayers
Drawbacks	Leaflet decoupling Uncompleted coverage (TR < 1) Defects (holes)	Symmetric bilayers Equilibrium lateral pressure non controlled	Symmetric bilayers Requires organic solvents Superimposed bilayers often obtained
Refs.	Rinia et al. (1999)	Richter et al. (2003)	Simonsen and Bagatolli (2004)

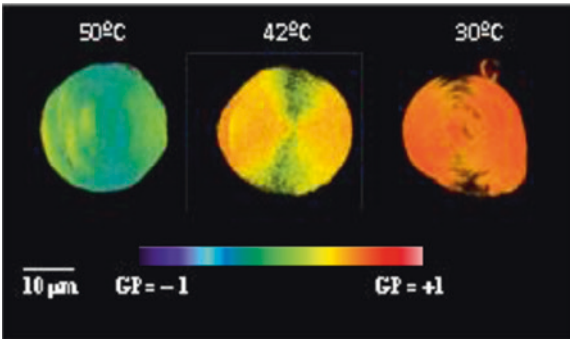


**Fig. 2.11** Two-photon microscopy with Laurdan-labeled DPPCGUVs:GP images of DPPC giant unilamellar vesicles (GUVs) stained with 5 μM Laurdan, in PBS at 50 °C (fluid phase), 42 °C (near the gel to liquid phase transition) and 30 °C (gel phase). Scale bar, 10 μm. GP images were pseudo colored with an arbitrary color palette (Generous gift from Dr. Carlos de la Haba, Dr. José Ramón Palacio, Dr. Paz Martínez and Dr. Antoni Morros)

confocal microscopy. There are several methods of preparation, which yield different sized, shapes and thickness (Bagatolli et al. 2000).

### 2.5.5 Bilayer Compressibility and Bilayer Surface Pressure

In this section several physical properties derived from the study of the elasticity of the bilayers are introduced. The modulus of compressibility ( $K_B$ ) of a bilayer is given by

$$K_B = V \left( \frac{\partial P}{\partial V} \right)_{T,n} \quad (2.16)$$

This expresses the response of the bilayer volume ( $V$ ) to the pressure ( $P$ ) at constant temperature ( $T$ ) and composition ( $n$ ). Similarly the modulus of surface compressibility ( $K_A$ ) is given by

$$K_A = A \left( \frac{\partial \bar{T}}{\partial A} \right)_{T,n} \quad (2.17)$$

that gives the response of the bilayer surface area ( $A$ ) to a tension ( $\bar{T}$ ) isotropically applied at constant  $T$  and  $n$ . Typical values of  $K_B$  and  $K_A$  for a fluid bilayer are  $(1-3) \times 10^9$  and  $0.14 \text{ N m}^{-1}$  respectively.

The curvature elasticity ( $B$ ) refers to the change of curvature of a surface in response to a bending moment ( $M$ ) acting on the bilayer edge

$$B = \left. \frac{\partial M}{\partial (1/R)} \right|_T \quad (2.18)$$

An important magnitude is the surface bilayer pressure ( $\pi_B$ ), that, contrarily to the surface monolayer pressure ( $\pi$ ), cannot be obtained experimentally. Indeed, it is interesting to know the equivalence between  $\pi$  and  $\pi_B$ . This can be done by investigating the isotherms of a given lipid at several temperatures and determining the  $T_m$  of the lipid of interest by plotting the molecular surface area as a function of the temperature and taking the maximum slope at a given pressure (Blume 1979). By using this method one finds that the  $\pi = \pi_B = 30 \text{ mN m}^{-1}$ . In this regard, using surface thermodynamics, one can write the equation for the mechanical equilibrium of the bilayer membrane as

$$\bar{T} = \gamma - \pi \quad (2.19)$$

where  $\gamma$  is the interfacial Gibbs energy density (equivalent to the hydrophobic surface energy density) and  $\pi$  is, the surface pressure in the bilayer. Since for large vesicles the isotropic tension has been demonstrate to be zero, (2.19) becomes

$$\gamma = \pi_0 \quad (2.20)$$

Then, taking a value of  $70 \text{ mN m}^{-1}$  for the hydrophobic Gibbs energy, one obtains a value for  $\pi_0$  for each of the two halves of the monolayer of  $35 \text{ mN m}^{-1}$ , which is in good agreement with the value of  $\pi_B$  discussed above.

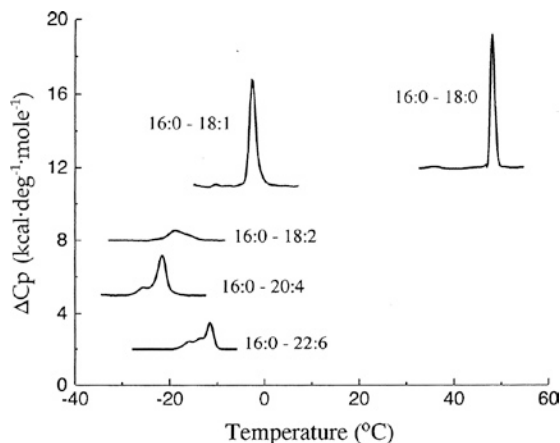
## 2.6 The Lipid-Phase Transition: Some Experimental Approaches

### 2.6.1 Differential Scanning Calorimetry of Lipids

In the presence of an excess of water, phospholipids form fully solvated lipid bilayers, which undergo a phase transition from the solid-like gel state ( $L_\alpha$ ) to the fluid liquid-crystalline state (called  $L_\alpha$ ) or liquid-disordered ( $L_d$ ) state at a temperature ( $T_m$ ) that is characteristic for each species and mixture. The value of  $T_m$  depends on the acyl chains composition, degree of unsaturation and the headgroup of the phospholipid. DSC measures heat flow into a sample as it is heated at a controlled rate over a range of temperatures, and can be used to measure the phase changes of liposomes. For DMPC and DPPC common phospholipids used in the laboratory, the values of  $T_m$  are 24 and 42 °C, respectively. The presence of an unsaturated acyl chain in the phospholipid structure produces a decrease in the  $T_m$ . Figure 2.12 shows the endotherms for a series of heteroacid phospholipids with the same headgroup, PC, a palmitic acid esterified at the *sn*-1 position and different unsaturated acyl chains at the *sn*-2 position (Hernandez-Borrell and Keough 1993). As can be seen POPC and PSPC show narrow endotherms with their  $T_m$  at -2 and 49 °C respectively. By increasing the number of double bonds from 1 to 6, the endotherm becomes more complex and the  $T_m$  value is decreased.

The lamellar  $L_\alpha$  (liquid crystalline) state is the most common state found in biological membranes and it is characterized by relative disorder in the acyl chain region in comparison to the lamellar  $L_\beta$  (gel) state. Most natural membranes contain a significant amount of unsaturated phospholipids that mixed with the other components maintain the natural membrane in the  $L_\alpha$  state. The transition to  $H_{II}$  phases can also be detected by using DSC. An example is the endotherm of POPE in presence of  $Ca^{2+}$  shown in Fig. 2.18a, where the transitions from  $L_\beta$  to the  $L_\alpha$  and from  $L_\alpha$  to the  $H_{II}$  are observed at 24.6 and 59.4 °C, respectively.

**Fig. 2.12** Endotherms for liposomes of PSPC (16:0–18:0), POPC (16:0–18:1), PLPC (16:0–18:2), PAPC (16:0–20:4) and PDPC (16:0–22:6). Redrawn from Hernandez-Borrell and Keough (1993) with permission from Elsevier Science



In the case of eukaryotic cell membranes, the presence of cholesterol in a given proportion results in bilayers showing intermediate properties between those of  $L_\beta$  and  $L_\alpha$  state, and for this reason the concept of a liquid-ordered ( $L_o$ ) phase has been introduced. This terminology is frequently associated with the literature on “Rafts” or detergent resistant membrane domains (DRMs) and when describing lipid phases of the lung surfactant.

Cholesterol causes a broadening of the endotherm and a decrease in the enthalpy of the transition whilst the  $T_m$  is gradually moved to lower values. The measureable change in the value of the enthalpy decreases as cholesterol concentration increases. The broadening of the transition and the loss of enthalpy correspond to a decrease in broad range of temperature. The amount of cholesterol required for the abolition of the enthalpy depends on each phospholipid species. In Fig. 2.13, for instance, 30% and 20 % mol/mol of cholesterol is required to abolish the enthalpy of the transition of PSPC and POPC, respectively. The thermal behavior of lipids is critical in the formation of vesicles in solution. Liposomes are normally prepared at a temperature above of the  $T_m$  of the selected phospholipid species because below its  $T_m$  the hydration of the lipid and its formation into liposomes is extremely (orders of magnitude) slower than for lipids above  $T_m$ . For this reason this process of forming closed vesicles may take minutes when the lipids are above  $T_m$  and even after hours of hydration below  $T_m$  fully sealed vesicles cannot be obtained.

### 2.6.2 Fluorescence Anisotropy

This method consists of measuring the anisotropic emission of fluorescent labels that are incorporated in the membranes. The fluorescence anisotropy values are calculated according to

$$r = \frac{I_{VV} - GI_{HV}}{I_{VV} + 2GI_{HV}} \quad (2.21)$$

where  $I_{VV}$  and  $I_{HV}$  are the intensities measured when polarizers are parallel and perpendicular to the exciting beam and  $G$  is the grating correction factor equal to  $I_{HV}/I_{HH}$ . In this technique, lipid-soluble fluorophores such as DPH (1,6-diphenyl-1,3,5-hexatriene) and TMA-DPH (trimethylammonium-DPH) with the ability to intercalate within the lipid bilayers are often used. DPH is a non-polar, but polarizable polyene that was the first molecule used to describe membrane fluidity/microviscosity. Fluidity is very low when the acyl chains are in the  $L_\beta$  phase and increases when the bilayer reaches the specific  $T_m$ . The relationship between the viscosity at a given temperature  $\eta(T)$  is given by

$$\eta(T) = \eta(T_m)^{-\Delta E\theta/RT} \quad (2.22)$$

where  $\theta = (T - T_m)/T_m$  is the reduced temperature and  $\Delta E$  the change in the energy during the transition.

While DPH shows a negligible fluorescence in water when it is added to lipid membranes it intercalates spontaneously within the acyl chains resulting in an increase of its fluorescence. When inserted in bilayers, DPH may exist in two orientations: one with its long axis parallel to the lipid acyl chains axes; and the other in the core of the bilayer, with its long axis parallel to the bilayer surface. DPH does not show preference either for the gel or for the fluid (liquid crystalline) phase. For TMA-DPH the DPH moiety is inserted between the lipid acyl chains, but due to its net positive charge, the TMA group lies in the water-lipid interface of the lipid bilayer, near the phospholipid head groups. When the lipid matrix in which the probe is embedded undergoes a transition between two phases, the anisotropy changes dramatically due to an increase (lower anisotropy) or decrease (higher anisotropy) of the membrane fluidity. These changes are easily measured using a conventional steady-state fluorimeter equipped with polarizers. Fluidity changes in different parts of the lipid bilayer due to phase transitions can also be tracked using different labels that show different localization in the membrane (as for example, DPH and TMA-DPH). In some cases, as in the study of the annular region around IMPs (Sect. 3.3) fluidity can also be assessed by using pyrene labeled phospholipids, by calculating the excimer-to-monomer ratio of this molecule. Pyrene is excited at 338 nm and two fluorescence maxima are obtained, at 375 and 470 nm, corresponding to the monomer and excimer bands, respectively.

After excitation by polarized light, the fluorescent dye experiences a free rotation during its fluorescent lifetime that is highly dependent on the membrane viscosity. Therefore, the degree of depolarization of the fluorescent emission versus the excitation light is intimately related with the degree of motion or fluidity in the lipid bilayer or, more precisely, with the fluidity of the microenvironment where the fluorophor is located. The fluorescent anisotropy value ( $r$ ) is calculated from the intensity of fluorescent emissions measured in different directions by using polarizers. Figure 2.14 shows the phase transition of synthetic lipid POPE:POPG (3:1, mol/mol) by following the fluorescent anisotropy decay of DPH at increasing temperatures. A sharp phase transition from  $L_\beta$  to  $L_\alpha$  can be observed corresponding to a sudden change in membrane fluidity. The following equation can be fitted to the anisotropy versus temperature data

$$r = r_1 + p_1 T + \frac{r_{s1} - r_{s2} + p_2 T - p_1 T}{1 + 10^{B\left(\frac{1}{T} - \frac{1}{T_m}\right)}} \quad (2.23)$$

where  $T$  is the absolute temperature,  $B$  is a measure of the cooperativity of the transition,  $p_1$  and  $p_2$  correspond to the slopes of the straight lines at the beginning and at the end of the plot, and  $r_1$  and  $r_2$  are the anisotropy intercepting values at the y axis. From  $r$  values the limiting anisotropy ( $r_\infty$ ) was determined using the following relationship

$$r^\infty = \frac{4}{3} r - 0.10 \quad (2.24)$$



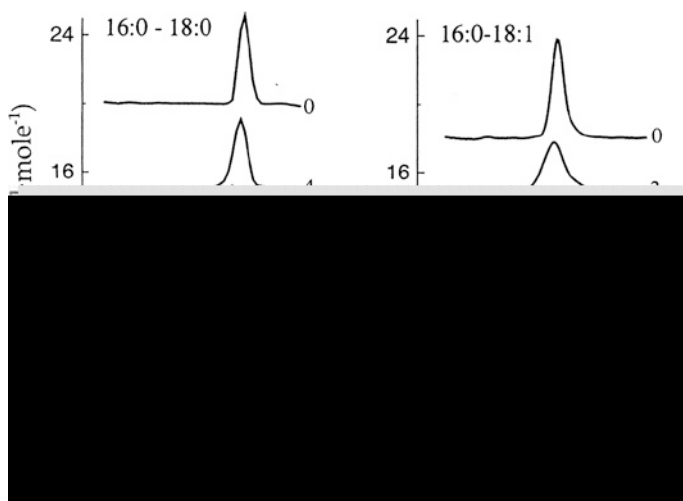


**Fig. 2.13** Endotherms of PSPC (*left*) POPC (*right*) liposomes in the presence of different amounts of cholesterol. Redrawn from Hernandez-Borrell and Keough (1993) with permission from Elsevier Science

**Fig. 2.14** Typical anisotropy curve of POPE:POPG (3:1) obtained by using DPH as a label

$r_{\infty}$  reflects restriction of probe motion and can be converted to an order parameter ( $S$ )

$$S^2 = \frac{r_{\infty}}{r^0} \quad (2.25)$$

where  $r^0$  is the fluorescence anisotropy in the absence of any rotational motion of the probe.

### 2.6.3 $^{31}\text{P}$ -Nuclear Magnetic Resonance Spectroscopy

$^{31}\text{P}$ -Nuclear magnetic resonance ( $^{31}\text{P}$ -NMR) spectroscopy provides a suitable technique in the study of the structural organization of biological membrane systems. This approach has the advantage that analysis is not disturbed by the presence of other non-phosphorus probe components.  $^{31}\text{P}$ -NMR has been successfully applied to study the conformation and dynamics of phospholipid head groups and also to detect lipid polymorphism.

NMR is sensitive to the angle that the molecules adopt with respect to the magnetic field. As a consequence, anisotropic samples produce broad signals. In order to reduce this effect, samples are submitted to rotation with respect to an axis which forms an angle of  $54.74^\circ$  with respect to the magnetic field. This is the so-called “magic angle” (MAS - Magic Angle Spinning) used in “solid-state” NMR. Membranes are anisotropic and moreover their samples possess a certain viscosity, originated by restriction in the molecular motion, which affects relaxation times. This is why most common phospholipids yield broad signals in their  $^{31}\text{P}$ -NMR spectra, with spectral widths ranging from 20 to 300 ppm depending on the meso-phase and hydration state of the sample.

In Fig. 2.15 the MAS  $^{31}\text{P}$ -NMR spectrum of MLVs of the saturated phospholipid DPPC registered at two temperatures is shown. The temperatures were chosen to be below ( $20^\circ\text{C}$ ) and above ( $54^\circ\text{C}$ ) the  $T_m$  of the phospholipid. A characteristic low field shoulder is visible mainly in the  $^{31}\text{P}$ -NMR spectrum for MLVs at the lower temperature. The transition from the  $L_\beta$  to the  $L_\alpha$  phase results in a spectral narrowing, which results in a decrease of the chemical shift dispersion, which is often attributed to the increase in the mobility of the phosphate groups. In the fluid state the observed narrower lineshape is attributed to the rapid rotation of lipids around the long axis of the molecule, which have a restricted motion around axes perpendicular to the rotating axis. These motional characteristics are determined by the disposition of the phospholipid molecules in a bilayer.

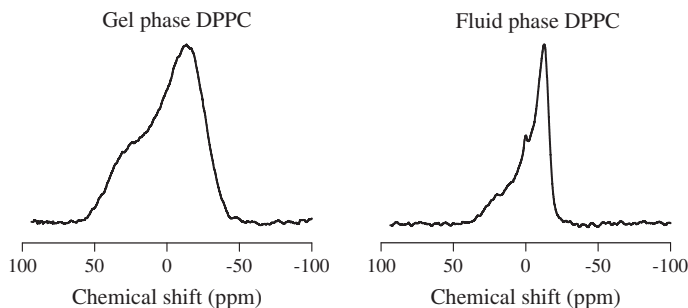


**Fig. 2.15**  $^{31}\text{P}$ -NMR spectra in the gel-phase ( $20^\circ\text{C}$ ) and in fluid phase ( $54^\circ\text{C}$ ) of DPPC multi-lamellar vesicles (MLV). Spectra were normalized to the same height. Unpublished results generously provided by Dr. Antoni Morros

Therefore, MAS  $^{31}\text{P}$ -NMR can be used as a suitable technique to detect the existence of a bilayer structure as well as to monitor the  $L_\beta$  to  $L_\alpha$  transition.

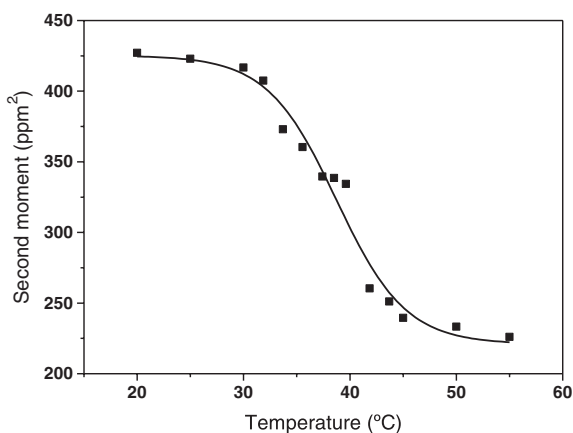
The chemical shift anisotropy (CSA) of the phosphorus atoms in phospholipids is a parameter frequently used to characterize the  $^{31}\text{P}$ -NMR spectra of phospholipids. It is calculated as the chemical shift difference between the high field peak and the low field shoulder. Since the  $^{31}\text{P}$ -NMR spectra of mixed liposomes do not always show a well-defined shoulder at low field, the determination of CSA directly from the powder pattern may not be accurate. Alternatively, the second moment ( $M_2$ ) of the powder pattern spectra, which can be accurately evaluated (Herreros et al. 2000), is determined.  $M_2$  values report on the square of the head-group order parameter and so reflect the changes occurring in the structure and dynamics of the phosphate headgroups (Léonard and Dufourc 1991; Gaillard et al. 1991). It is defined as

$$M_2 = \frac{\sum (w_i - M_1)^2}{\sum I_i} \quad (2.26)$$

where  $w_i$  and  $I_i$  are the frequency and intensity of the  $i$ th data point, respectively, and  $M_1$  is the first moment, which corresponds to the isotropic chemical shift of the sample. The short recycling delay used in these experiments ( $\text{TR} = 1.2 \text{ s}$ ) results in small differential saturation effects, that in turn translate into moderately overestimated  $M_2$  values with respect to those calculated from fully relaxed spectra ( $\text{TR} > 3 \text{ s}$ ).

Figure 2.16 shows the temperature dependence of the second spectral moment ( $M_2$ ) for DPPC. For DPPC a temperature increase leads to a monotonic decrease in  $M_2$  followed by a drastic decrease corresponding to the main transition temperature of the lipid bilayer which can be attributed to an increase in the local motions of phospholipid headgroups.

**Fig. 2.16** Temperature dependence of the second moment ( $M_2$ ) calculated from  $^{31}\text{P}$ -NMR spectra of DPPC multilamellar vesicles (MLV). Unpublished results generously provided by Dr. Antoni Morros



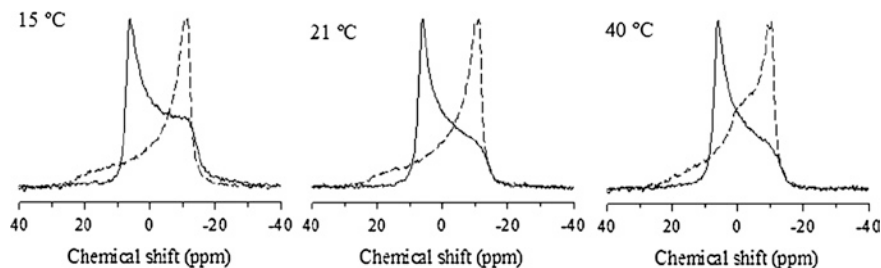


**Fig. 2.17** Solid-state  $^{31}\text{P}$ -NMR spectra at 15, 21 and 40 °C corresponding to POPE:CL (0.8:0.2, mol/mol) dispersions in  $\text{Ca}^{2+}$  free 50 mM Tris-HCl, pH 7.40, 150 mM NaCl buffer (*dashed line*), and in 20 mM  $\text{CaCl}_2$  added buffer (*continuous line*). Reprinted from Domènech et al. (2007b) with permission from Elsevier Science

$^{31}\text{P}$ -NMR spectroscopy is also an appropriate technique to unambiguously characterize the lamellar to  $H_{II}$  phase transition. Figure 2.17 shows the  $^{31}\text{P}$ -NMR powder pattern spectra of POPE:CL (0.8:0.2, mol/mol) systems at 15, 21 and 40 °C in the presence (continuous lines) and in the absence (dashed lines) of 20 mM  $\text{CaCl}_2$ . While, samples in the absence of  $\text{Ca}^{2+}$  show mainly the usual features of the lamellar phase, in the presence of calcium, the spectra show the typical shape corresponding to the  $H_{II}$  phase with the chemical shift dispersion having an “opposite” shape compared to the bilayer shape. At 15 °C the contribution of the lamellar phase was observed. This feature progressively disappears when temperature increases. In the  $H_{II}$  phase, there is a rapid diffusion of phospholipid along the cylinder axis which represents an additional mechanism of motional averaging (Domènech et al. 2007b).

#### 2.6.4 AFM in Force Spectroscopy (FS) Mode

AFM has been extensively used for topographic characterization of model membranes, and in particular, for identification and visualization of lipid domains and phase transitions in LBs (Oncins et al. 2007; Picas et al. 2008) and SLBs (Domènech et al. 2007a, b, c; Seeger et al. 2009). However, in cases where domains are not distinguished, phase transitions can be followed by monitoring the changes in the roughness of the surface at different temperatures. Accordingly DSC measurement (Fig. 2.18a) POPE SLBs present the  $L_\beta$  to the  $L_\alpha$  transition at 24.6 °C and the  $L_\alpha$ - $H_{II}$  transition at 59.4 °C. Topography changes are clearly apparent for these SLBs as shown in Fig. 2.18b.

AFM in force mode measurements are based on cantilever deflection as a function of the piezoelectric tube position where the sample is mounted and which is responsible for the upwards and downwards movement after applying a voltage. Noteworthy, the technique is commonly known as “force spectroscopy” (FS),

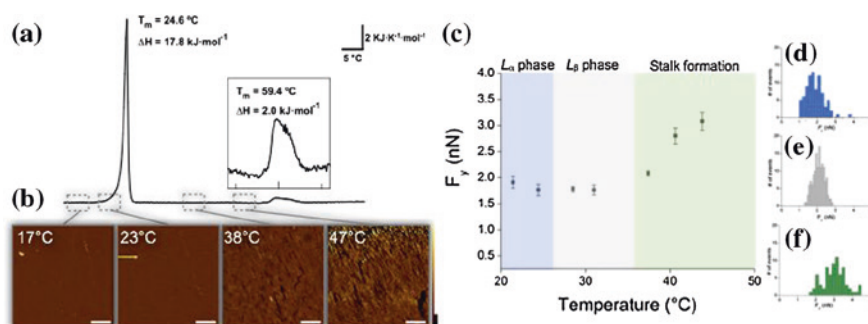


**Fig. 2.18** Endotherm of POPE containing 20 mM of  $\text{CaCl}_2$ , displaying the lamellar  $L_\beta$  to  $L_\alpha$  transition at 24.6 °C and the lamellar to hexagonal phase ( $H_{II}$ ) transition at 59.4 °C (a). AFM topography images acquired for POPE/POPE (30  $\text{mN m}^{-1}$ /25  $\text{mN m}^{-1}$ ) SLBs at different temperatures (17, 23, 38, and 47 °C) (b). Distribution of breakthrough forces ( $F_y$ ) obtained from  $F_vD$  curves performed at different temperatures for POPE/POPE (30  $\text{mN m}^{-1}$ /25  $\text{mN m}^{-1}$ ) SLBs (c), showing the different mechanical response upon changes in bilayer polymorphism. Representative histograms of the  $F_y$  variation as a function of the thermotropic state of POPE/POPE (30  $\text{mN m}^{-1}$ /25  $\text{mN m}^{-1}$ ) SLBs ( $L_\beta$  phase blue,  $L_\alpha$  phase grey, and stalk formation, green). Color scale is 20 nm and the bar scale is 1  $\mu\text{m}$ . Adapted from Picas et al. (2008)

even if there is no specific matter-radiation interaction. Two main items of information can be extracted from the FS curves: (i) the breakthrough or threshold force ( $F_y$ ), i.e. the force that the bilayer can withstand before being indented (ii) the adhesion force ( $F_{adh}$ ) between the tip and the bilayer. Actually, FS experiments are an interesting approach to reveal the nanomechanics behind the thermotropic behavior of lamellar phases. This introduces the possibility of studying other membrane systems and lipid polymorphisms following a similar approach. Thus the technique allows following the  $L_\beta$  to the  $L_\alpha$  and the  $L_\alpha$  to the  $H_{II}$  transitions of POPE though  $F_y$  measurements. In this particular experiment, within the temperature range, evaluation of breakthrough forces indicated a progressive increase in membrane resilience during transition from  $L_\alpha$  to  $H_{II}$  and the appearance of intermediate structures, known as stalks, at around 45 °C (Fig. 2.18c).  $F_y$  values are the average of the distributions shown in Fig. 2.18d–f. By using the same tips and experimental conditions, FS provides a means to unambiguously discriminate between phospholipid species and phases (Garcia-Manyes et al. 2010).

## References

- Bagatolli LA, Parasassi T, Gratton E. Giant phospholipid vesicles: comparison among the whole lipid sample characteristics using different preparation methods—a two photon fluorescence microscopy study. *Chem Phys Lipids*. 2000;105:135–47.
- Bangham AD, Standish MM, Weissmann G. The action of steroids and streptolysin S on the permeability of phospholipid structures to cations. *J Mol Biol*. 1965;13:253–9.
- Binnig G, Rohrer H, Gerber C, Weibel E. Surface studies by scanning tunneling microscopy. *Phys Rev Lett*. 1982;49:57–61.

- Blume A. A comparative study of the phase transitions of phospholipid bilayers and monolayers. *Biochim. Biophys. Acta—Biomembr.* 1979;557(1):32–44.
- Davies JTRE. *Interfacial Phenomena*. 1st ed. New York: Academic Press Inc.; 1963.
- Domènech Ó, Ignés-Mullol J, Teresa Montero M, Hernandez-Borrell J. Unveiling a complex phase transition in monolayers of a phospholipid from the annular region of transmembrane proteins. *J Phys Chem B*. 2007a;111(37):10946–51.
- Domènech Ò, Morros A, Cabañas ME, Teresa Montero M, Hernández-Borrell J. Supported planar bilayers from hexagonal phases. *Biochim Biophys Acta—Biomembr.* 2007b;1768(1):100–6.
- Domènech Ò, Redondo L, Picas L, Morros A, Montero MT, Hernández-Borrell J. Atomic force microscopy characterization of supported planar bilayers that mimic the mitochondrial inner membrane. *J Mol Recognit.* 2007c;546–53.
- Gaillard S, Renou JP, Bonnet M, Vignon X, Dufourc EJ. Halothane-Induced Membrane Reorganization Monitored by Dsc, Freeze-Fracture Electron-Microscopy and P-31-Nmr Techniques. *Eur Biophys J*. 1991;265–74.
- Garcia-Manyes S, Redondo-Morata L, Oncins G, Sanz F. Nanomechanics of lipid bilayers: Heads or tails? *J Am Chem Soc*. 2010;132(14):12874–86.
- Gennis RB. *Biomembranes : molecular structure and function*. Barcelona [etc.] : Springer; 1989.
- Groves JT, Boxer SG. Micropattern formation in supported lipid membranes. *Acc Chem Res*. 2002;35:149–57.
- Hernandez-Borrell J, Keough KM. Heteroacid phosphatidylcholines with different amounts of unsaturation respond differently to cholesterol. *Biochim Biophys Acta*. 1993;1153(2):277–82.
- Herreros B, Metz AW, Harbison GS. Moment analysis as a systematic tool for NMR powder pattern analysis. *Solid State Nucl Magn Reson*. 2000;16:141–50.
- Hoenig D, Moebius D. Direct visualization of monolayers at the air-water interface by Brewster angle microscopy. *J Phys Chem [Internet]*. 1991;95:4590–2. Available from: <http://pubs.acs.org/doi/abs/10.1021/j100165a003>.
- Israelachvili JN, Mitchell DJ, Ninham BW. Theory of self-assembly of hydrocarbon amphiphiles into micelles and bilayers. *J Chem Soc Faraday Trans.* 1976; 2:1525.
- Léonard A, Dufourc EJ. Interactions of cholesterol with the membrane lipid matrix. A solid state NMR approach. *Biochimie*. 1991;73:1295–302.
- Maget-Dana R. The monolayer technique: a potent tool for studying the interfacial properties of antimicrobial and membrane-lytic peptides and their interactions with lipid membranes. *Biochim Biophys. Acta—Biomembr.* 1999.
- Nag K, Keough KM. Epifluorescence microscopic studies of monolayers containing mixtures of dioleoyl- and dipalmitoylphosphatidylcholines. *Biophys J*. 1993;65(3):1019–26.
- Oncins G, Oncins G, Picas L, Picas L, Hernandez-Borrell J, Hernandez-Borrell J, et al. Thermal response of Langmuir-Blodgett films of dipalmitoylphosphatidylcholine studied by atomic force microscopy and force spectroscopy. *Biophys J*. 2007;93:2713–25.
- Pérez-Gil J. Structure of pulmonary surfactant membranes and films: The role of proteins and lipid-protein interactions. *Biochim. Biophys. Acta—Biomembr.* 2008;1778:1676–95.
- Peters R, Beck K. Translational diffusion in phospholipid monolayers measured by fluorescence microphotolysis. *Proc Natl Acad Sci*. 1983;80(23):7183–7.
- Petty MCM. *Langmuir-Blodgett films: an introduction*. Cambridge: Cambridge Univ Press; 1996.
- Picas L, Milhiet PE, Hernández-Borrell J. Atomic force microscopy: a versatile tool to probe the physical and chemical properties of supported membranes at the nanoscale. *Chem Phys Lipids*. 2012;845–60.
- Richter RP, Him JLK, Brisson A. Supported lipid membranes. *Mater Today*. 2003; 32–7.
- Rinia HA, Demel RA, van der Eerden JP, de Kruijff B. Blistering of langmuir-blodgett bilayers containing anionic phospholipids as observed by atomic force microscopy. *Biophys J*. 1999;77:1683–93.

- Schurch S, Lee M, Gehr P. Pulmonary surfactant: Surface properties and function of alveolar and airway surfactant. *Pure Appl Chem*. 1992;1745–50.
- Seeger HM, Marino G, Alessandrinia, Facci P. Effect of physical parameters on the main phase transition of supported lipid bilayers. *Biophys J Biophys Soc*. 2009;97(4):1067–76.
- Simonsen AC, Bagatolli LA. Structure of spin-coated lipid films and domain formation in supported membranes formed by hydration. *Langmuir*. 2004;20:9720–8.
- Tanaka M, Sackmann E. Polymer-supported membranes as models of the cell surface. *Nature*. 2005;437:656–63.
- Verger R, Mieras MCE, De Haas GH. Action of phospholipase A at interfaces. *J Biol Chem*. 1973;248:4023–34.

Membrane Protein – Lipid Interactions: Physics and  
Chemistry in the Bilayer

Borrell, J.H.; Domènech, Ò.; Keough, K.

2016, XIV, 116 p. 66 illus., 43 illus. in color., Softcover

ISBN: 978-3-319-30275-1